

A comprehensive preclinical study supporting clinical trial of oncolytic chimeric poxvirus CF33-hNIS-anti-PD-L1 to treat breast cancer

Shyambabu Chaurasiya,¹ Annie Yang,¹ Zhifang Zhang,¹ Jianming Lu,¹ Hannah Valencia,¹ Sang-In Kim,¹ Yanghee Woo,¹ Suanne G. Warner,² Tove Olafsen,³ Yuqi Zhao,⁴ Xiwei Wu,⁴ Seymour Fein,⁵ Linda Cheng,⁵ Maria Cheng,⁵ Nicholas Ede,⁶ and Yuman Fong¹

¹Department of Surgery, City of Hope National Medical Center, Familian Science building, Room#1100 1500 E Duarte Road, Duarte, CA 91010, USA; ²Department of Surgery, Mayo Clinic, Rochester, MN 55902, USA; ³Small Animal Imaging Core, Shared Resources, City of Hope National Medical Center, Duarte, CA 91010, USA; ⁴Integrative Genomics Core, City of Hope National Medical Center, Duarte, CA 91010, USA; ⁵CNF Pharma LLC, New City, NY 10956, USA; ⁶Imugene Ltd, Sydney, NSW 2000, Australia

CF33-hNIS-anti-PD-L1 is an oncolytic chimeric poxvirus encoding two transgenes: human sodium iodide symporter and a single-chain variable fragment against PD-L1. Comprehensive preclinical pharmacology studies encompassing primary and secondary pharmacodynamics and biodistribution and safety studies were performed to support the clinical development of CF33-hNIS-anti-PD-L1. Most of the studies were performed in triple-negative breast cancer (TNBC) models, as the phase I trial is planned for patients with TNBC. Biological functions of virus-encoded transgenes were confirmed, and the virus demonstrated anti-tumor efficacy against TNBC models in mice. In a good laboratory practice (GLP) toxicology study, the virus did not produce any observable adverse effects in mice, suggesting that the doses proposed for the clinical trial should be well tolerated in patients. Furthermore, no neurotoxic effects in mice were seen following intracranial injection of the virus. Also, the risk for horizontal transmission of CF33-hNIS-anti-PD-L1 was assessed in mice, and our results suggest that the virus is unlikely to transmit from infected patients to healthy individuals. Finally, the in-use stability and compatibility of CF33-hNIS-anti-PD-L1 tested under different conditions mimicking the clinical scenarios confirmed the suitability of the virus in clinical settings. The results of these preclinical studies support the use of CF33-hNIS-anti-PD-L1 in a first-in-human trial in patients with TNBC.

INTRODUCTION

Oncolytic viruses are designed to specifically replicate in cancer cells and kill them while leaving normal cells unharmed. A wide variety of viruses, either modified or in their natural form, have been studied for their oncolytic potentials. Many oncolytic viruses have been studied in clinical trials for the treatment of different types of malignancies.¹ Thus far, only one oncolytic virus, talimogene laherparepvec (T-Vec), has received U.S. Food and Drug Administration (FDA) approval. T-Vec, which is approved for the treatment of metastatic melanoma,

is an engineered herpes simplex virus 1 (HSV-1) that is armed with the cytokine granulocyte macrophage colony-stimulating factor (GM-CSF).² The approval of T-Vec has resulted in a surge of interest in the field of oncolytic virotherapy.

In addition to direct cell lysis, oncolytic viruses also rely on activation of anti-tumor immunity for their efficacy.^{3,4} It is therefore not surprising that oncolytic viruses show better efficacy when combined with other therapeutics that are known to avert immune suppression, such as the immune checkpoint inhibitors (ICIs).⁴ Backed by robust preclinical data, many clinical trials are ongoing in which oncolytic viruses are being tested in combination with checkpoint inhibitors.¹ Although most of these studies are still ongoing, results available from a few completed studies show that the combination of oncolytic virus and ICIs works well in patients. In phase I clinical trials, T-Vec with ipilimumab (a cytotoxic T lymphocyte-associated antigen 4 [CTLA-4] monoclonal antibody [mAb]) or pembrolizumab (a programmed cell death protein 1 [PD-1] mAb) has shown excellent efficacy in melanoma patients.^{5,6} Consequently, several ongoing phase II trials are evaluating T-Vec in combination with ICIs for the treatment of different types of malignancies.¹

Currently, T-Vec and ICIs cost well over \$100,000 each for one course of treatment.^{7,8} Given the high costs of ICIs, it will be beneficial to arm oncolytic viruses with transgenes encoding for ICIs. With this in mind, we have engineered a poxvirus, CF33, to encode a single-chain variable fragment (scFv) against programmed death ligand-1 (PD-L1). Furthermore, we have also armed this virus with human sodium iodide symporter (hNIS) gene, which would allow tracking of the

Received 16 September 2021; accepted 4 December 2021;
<https://doi.org/10.1016/j.omtm.2021.12.002>.

Correspondence: Shyambabu Chaurasiya, PhD, Department of Surgery, City of Hope National Medical Center, Familian Science building, Room#1100 1500 E Duarte Road, Duarte, CA 91010, USA.

E-mail: schaurasiya@coh.org

Table 1. Genome size and percentage identity of CF33 genome with those of parental viruses

Viruses	Genome Size, bp	Identities of CF33 to Genome, %	CF33 Coverage, %
CF33	189,415	100	100
VACV CL	184,042	99.24	95
VACV LC	190,579	99.00	97
VACV AS	177,923	99.19	88
VACV WR	194,711	99.38	97
VACV IHDW1	195,821	99.12	99
VACV Lister	187,893	99.22	96
Cowpox	224,499	97.54	99
Rabbitpox	197,731	99.32	99
Raccoonpox	214,699	87.04	83

virus *in vivo* using positron emission tomographic (PET) imaging.⁹ To support the testing of this doubly armed oncolytic virus, CF33-hNIS-anti-PD-L1 (also called HOV-3), in a phase I trial in patients with triple-negative breast cancer (TNBC), we have performed pre-clinical pharmacology studies encompassing primary and secondary pharmacodynamics and biodistribution and safety studies.

RESULTS

Sequence analysis of CF33

CF33 is a chimeric poxvirus generated through homologous recombination among nine strains/species of poxviruses.¹⁰ Simple alignment of CF33 genome sequence with the nine parental viruses shows that the Western Reserve (WR) strain of vaccinia virus (VACV) has the highest similarity (99.38%), while raccoonpox has the lowest similarity (87.04%) to CF33 (Table 1; Figure 1). Also, rabbitpox, IHD, and cowpox demonstrate the highest coverage (>99%) compared with the other six viruses (Table 1). However, it is hard to determine the origins of the CF33 genome regions from simple alignment. Therefore, we applied Kalign¹¹ to CF33 and the nine parental viruses for multiple sequence alignments. Previously, we had performed the sequence analysis of CF33 using only seven parental viruses whose sequences were publicly available.¹⁰ However, we recently performed sequencing of the remaining two parental viruses (VACV CL and VACV LC), and here we report the results of re-analysis of CF33 genome sequence compared against all nine parental viruses. The identities were calculated and viewed in SnapGene (Figure 2). The whole CF33 genome (189,415 bp) can be resolved into 41 segments, ranging from 353 to 40,691 bp. These segments were found to be derived mainly from three VACV strains: IHD, Lister, and WR, accounting for 60% of the whole CF33 genome. No sequence from raccoonpox or cowpox was detected in CF33 genome.

Poxvirus genes known to directly or indirectly play a role in attachment, entry, replication, and pathogenesis of virus were identified from the literature, and those genes in CF33 were mapped to the nine parental viruses. Our data show diverse parental origin of those

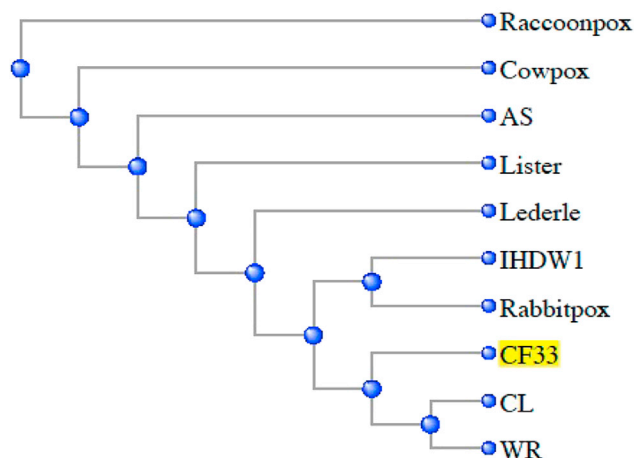


Figure 1. Phylogenetic tree of ten viruses created using the National Center for Biotechnology Information's (NCBI) multiple sequence alignment tool

genes (Table S1). Ten of 15 pathogenesis-related genes (C21L, C21L, A46R, A52R, SPI-2/CrmA, B18R, C12L, N1L, B8R, and E3L)¹² originated from the IHD strain of VACV. Interestingly, the entry genes came mainly from Lister and WR (10 of 11), such as I2L and J5L from Lister and G9R and L1R from WR. Moreover, genes involved in DNA replication, cell-cell fusion, and attachment were found to originate mainly from IHD and WR, such as A50R (DNA ligase) and D5R (helicase-primase), which originated from IHD and WR, respectively. Furthermore, genes involved in nucleotide metabolism (F4L, A48R, and J2R) are derived from the IHD strain.

In-use stability and device compatibility of CF33-hNIS-anti-PD-L1

We performed studies to determine stability of the virus at room temperature and on ice after thawing. We also determined the stability of virus after multiple freeze-thaw cycles. Furthermore, we determined the stability of the virus in a delivery device (i.e., syringe) for up to 2 h. The virus shows excellent stability at all the conditions tested except in the freeze-thaw cycle study with the lower concentration (1E6 plaque-forming units [PFU]/mL) of the virus (Figures 3A–3C). It was surprising that the virus at high concentration (1E08 PFU/mL) showed no change in titer for up to five freeze-thaw cycles, whereas the same virus at lower concentration (1E06 PFU/mL) showed drastic reduction in titer after every freeze-thaw cycle (Figure 3B). The reason for this discrepancy is not known.

In order to determine the genome stability of the virus during passaging, we sequenced virus genome after every round of passaging for up to five passages (P). Of the five samples (P1–P5), DNA from P2 sample was somehow degraded, and hence sequencing was not performed on the P2 sample. PacBio sequencing was performed on P1, P3, P4, and P5 samples. For analysis, sequence of P1 was used as reference sequence to compare sequences from P3, P4, and P5 to determine the extent of mutations in those late passages of virus. Results of the analysis are shown in Table 2. The comparison between P1

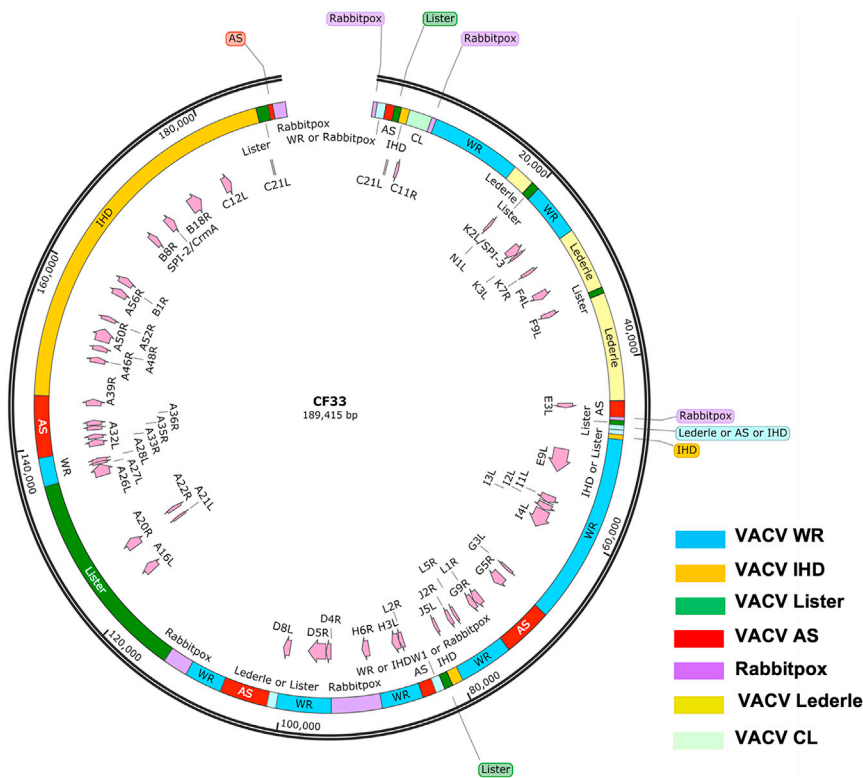


Figure 2. Genomic analysis of CF33

Map of virus genome showing components of parental viruses. Genomic regions are colored according to their parental viruses. Also shown are the origin of genes involved in attachment (A26L, H3L, D8L, and A27L), entry (A21L, G3L, H2R, A28L, F9L, L5R, I2L, J5L, A16L, G9R, and L1R), nucleotide metabolism (F4L, I4L, J2R, and A48R), DNA replication (G5R, E9L, I1L, A20R, A32L, A50R, B1R, D4R, H6R, I3L, D5R, and A22R), prevention of super-infection (A33R and A36R), cell-cell fusion (A56R and K2L), and pathogenesis (A39R, A35R, C21L, A46R, A52R, CrmA, E3L, K3L, K7R, N1L, C11R, B8R, and B18R).

CF33-hNIS-anti-PD-L1. In the murine normal cell line EpH4-EV, both CF33 and CF33-hNIS-anti-PD-L1 have lower replication compared with the WR and IHD strains of VACV. Again, the Lister strain has reduced replication in this cell line. Finally, CF33-hNIS-anti-PD-L1 was found to have no replication in NIH3T3 cells at any time point (Figure 4).

Toxicology and biodistribution study

A GLP toxicology study was performed by a third party (Comparative Biosciences, Inc) to determine the toxicity and biodistribution of

(Seed Stock) and its passages (P3, P4, and P5) indicated two variances (locations 437 and 438) shared among the three passages (Table 2). These two variants occurred within or near homopolymer regions, and it has been reported that deletion sequencing errors are very common in homopolymer regions with PacBio sequencing.¹³ However, these two variants shared among three samples tend to be real. Therefore, to determine if the two variants may alter gene expression, P1 assembly was annotated using VGAS, resulting in 272 genes ranging from 126 to 3,495 bp. Sequence of these genes were aligned against P3, P4, and P5 assemblies using Blast. The results show that these genes are conserved (100% sequence similarity) among the four passages (data not shown). Hence, the two variants are not likely to cause any alteration in the biological function of gene products.

Replication of CF33-hNIS-anti-PD-L1 is attenuated in normal cells

We compared the replication kinetics of the virus with that of parental strain (CF33) as well as with the three wild-type strains (IHD, Lister, and WR), which constitute the majority of the CF33 genome. Compared with CF33, replication of CF33-hNIS-anti-PD-L1 virus was found to be about 1 log lower in the human normal cell lines HDFa and Hs27 at all three time points tested (Figure 4). Also, replication of CF33-hNIS-anti-PD-L1 was lower than the wild-type viruses (Lister, IHD, and WR) in both human cell lines except for the Lister strain in Hs27 cells. The Lister strain of VACV seems to have reduced replication in Hs27 cells, to a level similar to

CF33-hNIS-anti-PD-L1 in an orthotopic syngeneic murine model using C57Bl/6 mice implanted with E0771 cells. The objectives of the study were to assess (1) toxicity and biodistribution of a single intratumorally (i.t.) administered CF33-hNIS-anti-PD-L1 in tumor-bearing mice in 3 weeks and (2) toxicity and biodistribution of repeated intratumorally administered CF33-hNIS-anti-PD-L1 in tumor-bearing mice in 12 days and after a 9 day recovery. The study consisted of 25 groups of C57Bl/6 mice: groups 1–7 for toxicology (histopathology), groups 8–14 for tissue biodistribution, groups 15–19 for serum troponin assays, and groups 20–25 for serum cytokine assays (Tables S2–S5). Virus at 1E03, 1E04, or 1E05 PFU was used for single or repeat injections. The highest dose (1E05 PFU) in mice would translate to approximately 5E08 PFU. These doses were chosen to allow testing of virus doses ranging from 1E06 to 5E08 PFUs in humans.

In the 3 week study period, no virus-related abnormalities were found in daily clinical observations or weekly body condition scores. Furthermore, once- or twice-weekly measurements of body weight, food consumption, and tumor size showed no statistically significant differences in males or females among the single-dose groups (groups 1–4) or among the repeat-dose groups (groups 5–7) (data not shown).

Blood levels of cytokines, IFN-g, IL-1b, IL-6, IL-10, TNF-a, and TGF-β1, were tested at 3 h, day 7, and day 14 in the single-dose groups and at days 14, 19, and 21 in the repeat-dose groups. There were no

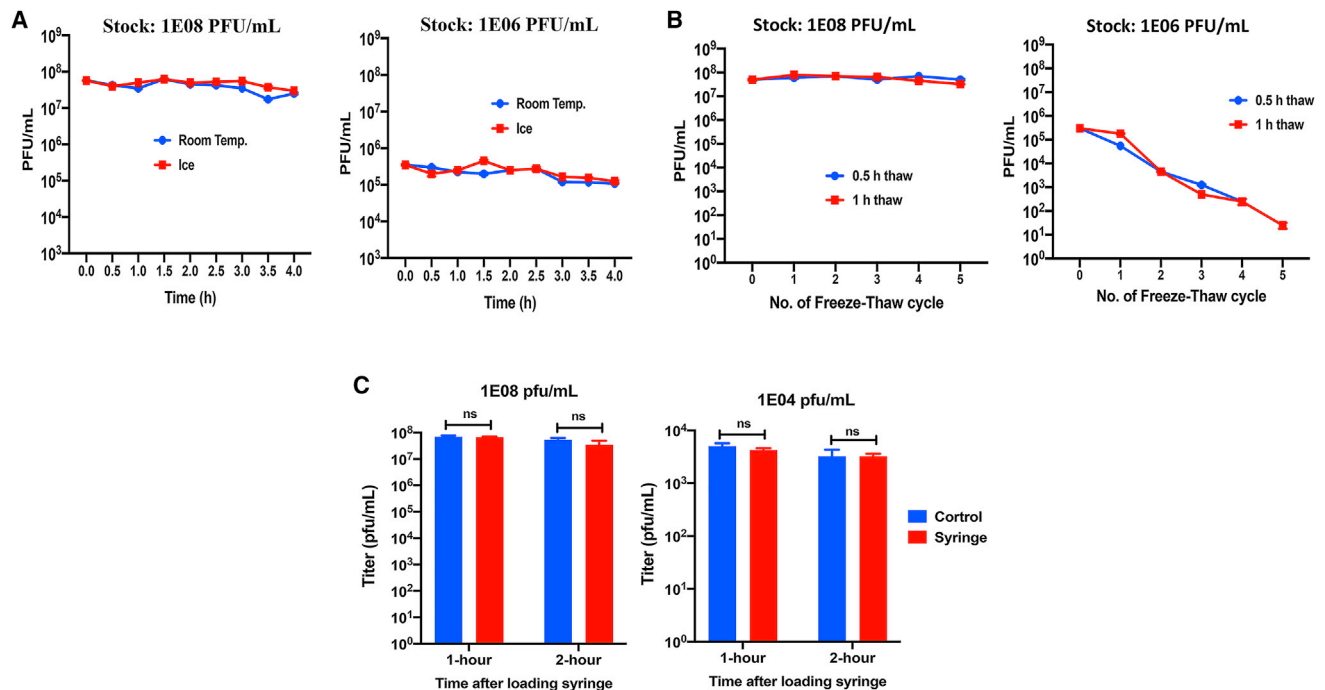


Figure 3. Stability of CF33-hNIS-anti-PD-L1

(A) CF33-hNIS-anti-PD-L1 at 1E08 or 1E06 PFU/mL was thawed and placed either at room temperature (RT) or on ice. Aliquots from all vials were taken immediately after thawing (0 h) and at 0.5, 1, 1.5, 2, 2.5, 3, 3.5, and 4 h. At each time point, aliquots of virus taken from the vials were immediately used to infect CV-1 cells for titration. Mean \pm SD is plotted. (B) Stability of CF33-hNIS-anti-PD-L1 after multiple freeze-thaw cycles. Virus stocks at 1E08 or 1E06 PFU/mL were freeze-thawed for up to five cycles (frozen for 1 h at -80°C and thawed for 30 min or 1 h at RT). After every thaw, aliquots were taken and immediately used to infect CV-1 cells for titration. Mean \pm SD is plotted. (C) Stability of the virus in syringe. Viruses at 1E08 or 1E04 PFU/mL were loaded in 10 mL syringes fitted with 25G needles and incubated for 1 or 2 h at RT. At the end of 1 and 2 h incubation, virus was ejected from the syringes and immediately used to infect CV-1 cells for titration. Virus incubated at room temperature in an Eppendorf tube was used as control.

changes in the cytokine levels compared with vehicle controls except that TGF- β 1 levels were significantly higher in the repeat-high-dose group at all time points compared with the vehicle control group (Tables S6–S10). Cardiac troponin I levels were below the limit of quantification (<7.82 pg/mL) in all samples.

For histopathological examinations, mice were euthanized at 24 h, 7 days, and 21 days after treatment for single-dose groups (groups 1–4) and at 12 and 21 days after first injection for repeat-dose groups (groups 5–7). Tissues included in the histopathological study were: adrenal gland, artery, aorta, femur, bone marrow, sternum, brain, esophagus, eye, heart, intestines, cecum, colon, duodenum, ileum, jejunum, kidney, liver with gall bladder, lung, lymph node, mandibular and mesenteric lymph nodes, muscle, hindlimb, sciatic nerve, oral tissues, tongue, ovary with oviduct, pancreas, salivary gland, skin, spinal cord, spinal cord with cervical portion, spinal cord with lumbar portion, thorax, spleen, stomach, thymus, thyroid with parathyroid, trachea, tumor, urinary bladder, uterus, and vagina. From histopathology examination, no virus-related microscopic findings were detected in any of the treatment groups, and the pathologist concluded that CF33-hNIS-anti-PD-L1 was well tolerated at all doses tested.

Biodistribution of virus was assessed using two techniques: (1) standard plaque assay and (2) quantitative PCR (qPCR) in groups 8–14 (Table 3). Tissues and samples used for biodistribution studies were: blood, urine, feces, saliva, bladder, brain, heart, intestine, kidney, liver, lung, muscle, ovaries, spleen, and tumors.

Among the 15 tissue and sample types tested by qPCR, the only sample showing the presence of viral DNA was tumor. Specifically, viral DNA was detectable in two of five tumor samples at day 7 and 0 of 5 samples at days 19 and 21 in the single-high-dose group. In the repeat-high-dose group, viral DNA was also detectable in 3 of 5 tumor samples at day 12 and 1 of 5 samples at days 19 and 21. None of the tumor samples in the vehicle control groups had detectable viral DNA. Data from the qPCR analysis for all organs are included in Table S11.

Among the 15 tissue and sample types tested in the standard plaque assay, infectious virus was detectable only in the tumor samples of the single-high-dose group (1 of 5; 500 PFU/g) at day 7 and repeat-high-dose group (2 of 5; 100 and 455 PFU/g) at day 12. The tumor samples at the later time points of these two groups and all the tumor samples in the vehicle control groups were found to be negative

Table 2. Detected variants from *de novo* assemblies (HOV-3 P3, P4, and P5)

Reference	Sample	Location	Type	Mismatched Base	Context
HOV-3 P1 (191,820 bp)	P3	437	substitution	T → A	AAATTT
		438	substitution	A → T	AAATTT
	P4	437	substitution	T → A	AAATTT
		438	substitution	A → T	AAATTT
	P5	437	substitution	T → A	AAATTT
		438	substitution	A → T	AAATTT

for infectious virus. The qPCR and plaque assay results suggest that after administration, the virus was specifically distributed in the administered tumors, and the levels in tumors decreased over time.

Assessment of neurotoxic effect of the virus

Wild-type vaccinia virus such as the WR strain has been shown to cause severe neurotoxicity in mice at a dose as low as 100 PFU^{14,15} when injected intracranially. In order to rule out the possibility of a neurotoxic effect of CF33-hNIS-anti-PD-L1, we used CF33-hNIS-anti-PD-L1 virus at a dose 10 times higher (1,000 PFU) than the dose reported to cause severe neurotoxicity for wild-type vaccinia virus. C57BL/6 mice of both genders were injected intracranially with 1,000 PFU CF33-hNIS-anti-PD-L1 virus or PBS as control. Mice were closely monitored for 30 days for signs of toxicity, and their body weights were measured daily. At the end of the observation period, mice were euthanized, and histopathological analysis was performed on their brains by a veterinary pathologist. No overt sign of toxicity was observed in the mice, and change in weight of the mice in virus-injected group was very similar to that for PBS-injected group (Figure 5). Furthermore, analysis of brain sections showed no virus-related adverse effects at the injection site. Also, away from the cerebellar injection region, brain sections of virus-treated animals looked very similar to those of the PBS-treated animals, suggesting that there was no virus replication in brain cells and hence no killing of brain cells by the virus. Taken together, these data show that CF33-hNIS-anti-PD-L1 does not have any clinically meaningful neurotoxic effect in mice at the dose tested.

Assessment of risk for horizontal transmission

The risk for horizontal transmission was also assessed for CF33-hNIS-anti-PD-L1 virus. To assess the risk, we injected E0771 tumor-bearing mice intratumorally with 1E06 PFU CF33-hNIS-anti-PD-L1 and then housed them with other mice, with or without tumors, that were not injected with virus, as shown in Figure 6A. The dose of virus used in this study was chosen at 10-fold higher than the highest dose used in the toxicology study, to rule out the possibility of virus transmission from injected to non-injected mice. To mimic the clinical situation in which patients receiving CF33-hNIS-anti-PD-L1 would be isolated for at least 24 h, we isolated virus-injected mice for 24 h in a separate cage. Following the 24 h isolation, virus-injected and non-injected mice were housed together such that each cage had at least one mouse that had been injected with virus. Finally, virus titers were measured in the

tumors and normal tissues of all mice from a cage at day 7, day 14, and day 21, to determine whether the virus could be detected from non-injected mice. Our results indicate that the CF33-hNIS-anti-PD-L1 virus did not transmit from injected to non-injected mice, as no virus was detected in tumor or tissues of non-injected mice. Also, even in the injected mice, virus was detectable only in the tumors. Furthermore, no virus was detected even in injected tumor at 3 weeks post-injection (Figure 6B), suggesting that virus may have been completely cleared by the immune system at this time point.

Transgenes in CF33-hNIS-anti-PD-L1 make functional proteins

The anti-PD-L1 cDNA in the virus is composed of an Igk light chain leader sequence, the VH chain sequence of an anti-PD-L1 monoclonal antibody, a (G4S)₃ linker sequence, the VL chain sequence, and a C-terminal FLAG tag (DDDDK tag). The anti-PD-L1 expression cassette is under the control of the vaccinia H5 promoter. First, we used Western blot analysis to detect the expression of anti-PD-L1 from virus-infected breast cancer cells (Figure 7A). We then evaluated the ability of virus-encoded anti-PD-L1 to block PD-L1 on the surface of human and murine breast cancer cells. Mouse breast cancer cells, E0771, were pre-incubated with purified virus-encoded anti-PD-L1 or control antibody (atezolizumab), followed by staining with anti-mouse PD-L1-PE antibody. Cells were then analyzed using flow cytometry. Our results demonstrate that virus-encoded anti-PD-L1 scFv blocks the detection antibody from binding to PD-L1 on mouse breast cancer cells E0771, in a dose-dependent manner (Figure 7B). Similar results were found against the human breast cancer cell line MDA-MB-468 (data not shown).

Expression of the transgene hNIS and localization of the protein on cell surface was confirmed using immunofluorescent staining of hNIS *in vitro* (Figure 7C). Immunofluorescence staining was performed 24 h after infection of cells at a multiplicity of infection (MOI) of 0.01.

CF33-hNIS-anti-PD-L1 favorably modulates immune cells and exhibits anti-tumor efficacy in the murine syngeneic model E0771

Mice bearing E0771 tumors were injected with a single intratumoral injection of 1E05, 1E06, or 1E07 PFU CF33-hNIS-anti-PD-L1 or PBS and euthanized 7 days later. Tumor volume and weight of mice were measured before treatment and immediately before euthanasia. No

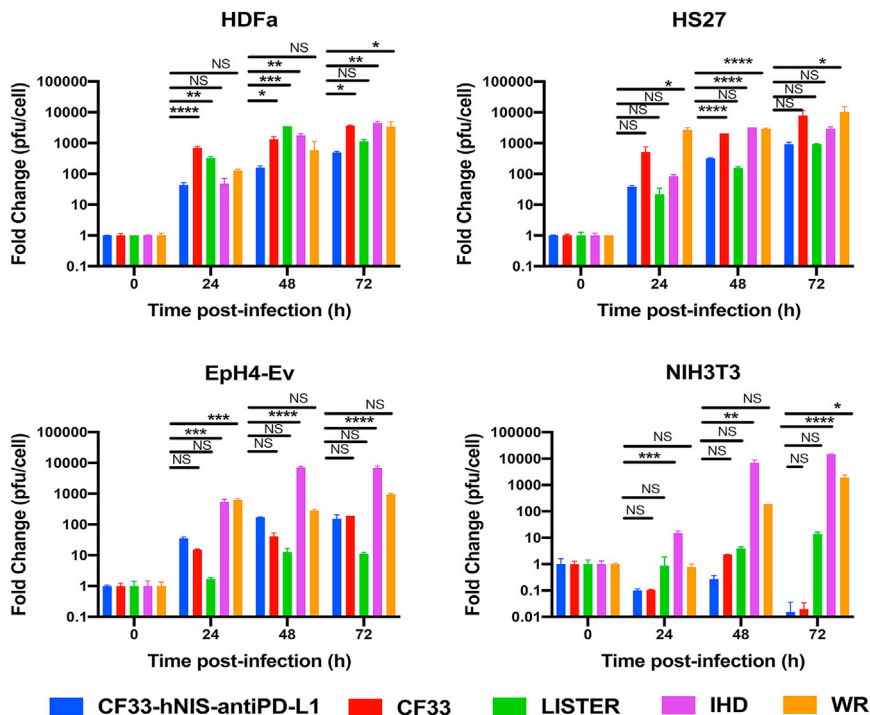


Figure 4. Replication of viruses in normal cells

Normal cell lines of human (HDFa and HS27) or murine (Eph4-Ev and NIH3T3) origin were infected with the indicated viruses at an MOI of 0.01, and virus titers were determined at indicated time points. Fold change in PFU/cell was calculated by dividing the virus titers at different time points with the titer of virus used for infection. Mean ± SD is plotted.

significant difference was observed between the average weight of mice treated with PBS and any of the virus doses (Figure 8A). Average tumor volume for virus-treated groups were less than the PBS-treated group (Figure 8B) over the 1 week time period, but because of high variation within the PBS group the difference did not reach statistical significance.

Tumors harvested 1 week post-treatment were divided into two parts; one part was used for immune cell analysis using flow cytometry and the other part for quantification of anti-PD-L1 and CF33-hNIS-anti-PD-L1 virus using qPCR. Interestingly, although there was a trend toward a higher amount of viral DNA in tumors treated with higher doses of virus, differences between the highest and lowest dose groups were not statistically significant (Figure 8C). As for the levels of anti-PD-L1, four of six mice in the lowest dose group (1E05 PFU), six of six mice in the mid-dose group (1E06 PFU), and five of six mice in the highest dose group (1E07 PFU) had detectable levels of anti-PD-L1. Although there was no significant difference in the levels of anti-PD-L1 between low and mid doses, the highest dose group had significantly higher levels of anti-PD-L1 (Figure 8D). The fact that anti-PD-L1 level was markedly different in mice treated with the highest dose suggests that the dose of virus needs to reach or exceed a certain threshold (1E07 PFUs in this case) to produce an abundant amount of product from their transgenes.

Immune cells were analyzed in tumor, blood and spleen and levels of different immune subsets were compared among the treatment groups. Levels of immune cells (CD45+) in the tumors treated with the highest dose (1E07 PFU) of the CF33-hNIS-anti-PD-L1 were

higher than those in PBS-treated tumors or tumors treated with lower doses of virus (Figure 9). However, because of large variation within treatment groups, the difference did not attain statistical significance. Interestingly, levels of CD8+ T cells were significantly higher in the tumors of the mid- and high-dose groups compared with the PBS group. Among the virus-treated groups, levels of CD8+ T cells seem to correlate with the doses of virus (Figure 9). Similar results were observed for blood and spleen (data not shown). Levels of PD-L1 in non-immune cells (CD45- cells, mostly tumor cells) were found to be significantly higher in the low-dose group compared with the PBS group (Figure 9), which is consistent with our previous findings that cancer cells upregulate PD-L1 expression in response to CF33 virus.¹⁶ However, compared with the low-dose group, the mid- and high-dose groups showed lower levels of PD-L1 in non-immune cells. This is probably due to blockade of PD-L1 by virus-encoded anti-PD-L1.

CF33-hNIS-anti-PD-L1 exhibits anti-tumor efficacy against 4T1 tumor model

In this study, we evaluated the safety and anti-tumor efficacy of CF33-hNIS-anti-PD-L1 in the highly aggressive 4T1 model. BALB/c mice bearing bilateral orthotopic tumors were injected with virus or PBS on days 1, 3, and 5 either intratumorally or intravenously (i.v.). Virus was injected (1E07 PFU) to each tumor, or 2E07 PFU was injected per mouse intravenously. The virus treatment was well tolerated in mice, as evidenced by weight change (Figure 10A). Both the i.t. and i.v. treatment with CF33-hNIS-anti-PD-L1 demonstrated some levels of anti-tumor efficacy and significantly increased survival of the virus-treated mice (Figures 10B and 10C).

CF33-hNIS-anti-PD-L1 shows excellent anti-tumor efficacy against a TNBC xenograft model

In order to test the efficacy of the virus against TNBC of human origin, we used a xenograft model in which tumors were generated in athymic mice using human TNBC cells MDA-MB-468. Mice were treated intratumorally with a single injection of CF33-hNIS-anti-PD-L1 at doses that were used in the toxicology study (1E03, 1E04, or 1E05 PFU) and were monitored for weight change as a surrogate of toxicity, and tumor regression for anti-tumor efficacy. In this study, mice treated

Table 3. Groups of mice used in biodistribution study

Group	Number/Sex of Mice	Animal Number (F)	Tumor Induction	Test Article Treatment	In-Life Procedure	Termination	Terminal Procedure	
8	5/F	851–855	Yes	i.t. 1 × day 0	control article (vehicle)	day 7	terminal blood and tissue collection for viral plaques and PCR	
	8/F	856–863				day 21		
9	5/F	951–955			CF33-hNIS-anti-PD-L1 1E03 PFU	day 7		
	8/F	956–963				day 21		
10	5/F	1051–1055			CF33-hNIS-anti-PD-L1 1E04 PFU	clinical observations: 1 × daily body condition scoring: weekly body weights: pre-study and necropsy		day 7
	8/F	1056–1063						day 21
11	5/F	1151–1155			CF33-hNIS-anti-PD-L1 1E05 PFU	pre-study and necropsy		day 7
	8/F	1156–1163						day 21
12	5/F	1251–1255			control article (vehicle)	pre-study and necropsy		day 12
	8/F	1256–1263						day 21
13	5/F	1351–1355			CF33-hNIS-anti-PD-L1 1E03 PFU	pre-study and necropsy		day 12
	8/F	1356–1363						day 21
14	5/F	1451–1455			CF33-hNIS-anti-PD-L1 1E05 PFU	pre-study and necropsy		day 12
	8/F	1456–1463						day 21

The table shows only female mice. The same number of male mice were also treated in the exact same manner.

with different doses of virus gained weight similarly to mice treated with the control (PBS) (Figure 11A). This suggests that all doses of CF33-hNIS-anti-PD-L1 used in this study were well tolerated. Furthermore, all three doses of CF33-hNIS-anti-PD-L1 virus were able to inhibit growth of the tumor (Figure 11B), indicating a robust anti-tumor potency of this virus against TNBC of human origin.

DISCUSSION

The objectives of these studies were to evaluate the risks and benefits of using the oncolytic virus CF33-hNIS-anti-PD-L1 to support clinical development in patients with TNBC. Because CF33 is a chimeric poxvirus generated from multiple species and strains of poxviruses, it was important to perform a thorough investigation of the viral genome and its stability. We compared the genome of CF33 with the genome of all nine parental viruses and determined the origin of sequences in CF33. The majority of the CF33 genome is derived from the vaccinia virus strains IHD, Lister, and WR, whereas no sequence from raccoonpox or cowpox was detected. Also, in CF33 most of the genes involved in viral DNA replication and pathogenesis are derived from the VACV strain IHD, which was used as a vaccine against smallpox.

Through a variety of experimental methods, we evaluated the safety associated with the use of the oncolytic virus. First, *in vitro* studies were performed to compare the growth of CF33-hNIS-anti-PD-L1 with CF33 and the parental viruses that make up the majority of CF33 genome (WR, Lister, and IHD) in normal cell lines of human and murine origins. CF33-hNIS-anti-PD-L1 showed attenuated replication compared with CF33 and other wild-type viruses, with the exception of the Lister strain. A GLP toxicology study performed by

a third-party company to determine the safety and biodistribution of CF33-hNIS-anti-PD-L1 in tumor bearing C57BL/6 mice treated with single or multiple injections of the virus at various dose levels showed no virus-related toxicity. Furthermore, intracranial injection of the virus at a dose 10 times higher than the lethal dose of WR strain^{14,15} in C57BL/6 mice did not show clinically meaningful virus-related toxicities. Finally, the risk for horizontal transmission of the virus using an experimental setup to mimic the clinical scenario suggested that the risk for horizontal transmission for this virus is minimal.

We evaluated the functionality of the virus-encoded transgene, anti-PD-L1, to confirm that the protein is biologically functional. Functionality of virus-encoded anti-PD-L1 was assessed using an *in vitro* competitive binding assay. Anti-PD-L1 protein purified from virus-infected cells showed a dose-dependent response in the assay, confirming the ability of virus-encoded protein to bind to PD-L1 on cell surface. However, compared with atezolizumab (an FDA-approved anti-PD-L1 mAb) virus-encoded anti-PD-L1 was found to be less effective. This could be partly because the virus-encoded antibody used in this study was not as pure as the atezolizumab. Nevertheless, this assay confirmed that the virus-encoded protein is functional.

Finally, we evaluated anti-tumor efficacy of the virus using xenograft and syngeneic models of TNBC in mice. It should be noted that higher doses of virus were used in syngeneic tumor models for efficacy studies than the doses used in toxicology studies, because murine tumors are less susceptible to the virus, but therapeutic doses in clinical trials will be based on the doses used in toxicology studies. In the E0771 tumor model, immune cell analysis 7 days after virus injection showed a

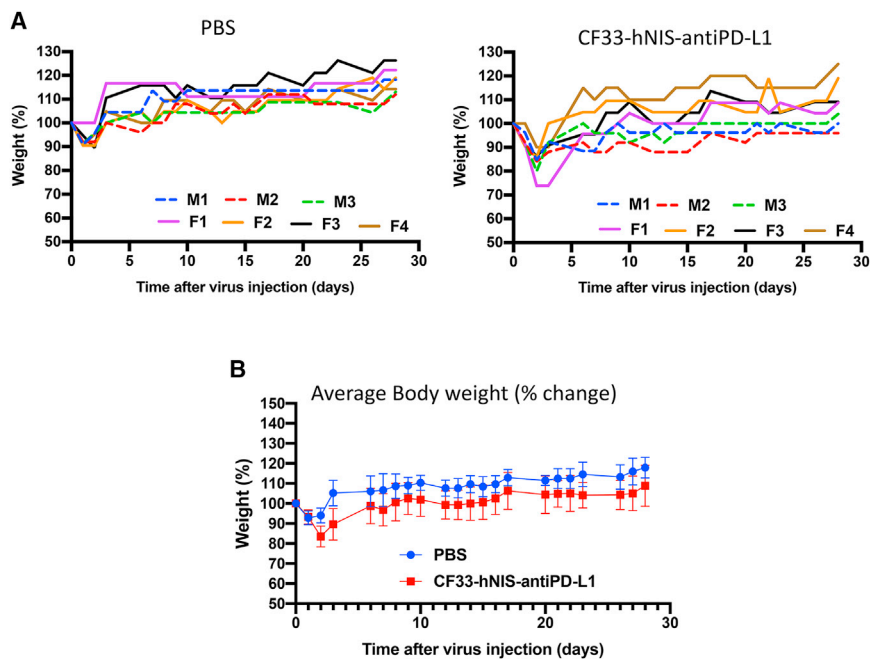


Figure 5. Assessment of neurotoxic effect of CF33-hNIS-anti-PD-L1

Male (M) and female (F) mice were treated intracranially with PBS or 1,000 PFU CF33-hNIS-anti-PD-L1, and their weight was measured every day and plotted. (A) weight of individual mouse in each treatment group is shown. (B) Average weight for each treatment group was plotted and compared. The difference between the two group is not statistically significant.

significantly larger number of CD8+ T cells in tumors of mice that were treated with virus compared with those treated with PBS. This increase in the number of CD8+ T cells in the tumors was found to be dose dependent, which is in agreement with a recently published study by Flores et al.¹⁷ in which the authors showed that a high dose of an oncolytic myxoma virus (1E06 foci-forming units [FFU]) resulted in a significant increase in CD8+ T cells in a melanoma model, whereas a low dose (1E04 FFU) of the same virus failed to do so. The fact that the virus was able to increase tumor infiltration by CD8+ T cells is indicative of positive immune modulation by the virus. However, despite positive immune modulation, the anti-tumor efficacies observed in these syngeneic models were modest. This was not surprising as we have previously shown that murine cancer cells are less susceptible to CF33 compared with human cancer cells.¹⁰ Furthermore, the two syngeneic models used in this study (4T1 and E0771) are extremely aggressive models that are difficult to control. Importantly, in a xenograft model of TNBC (MDA-MB-468), CF33-hNIS-anti-PD-L1 was able to completely control tumor growth at a dose as low as 10^3 PFU, a dose 100- to 1,000-fold lower than those reported for other oncolytic viruses.^{18–20} This shows the excellent efficacy of the virus against tumor of human origin.

Taken together, our data show that CF33-hNIS-anti-PD-L1 is a safe and low-risk virus with potent anti-tumor efficacy against TNBC of human origin, and thus these data support further evaluation of the virus in clinical settings.

MATERIALS AND METHODS

Virus

CF33 is a chimeric poxvirus generated through homologous recombination among nine strains/species of poxviruses. Construction of

CF33 and CF33-hNIS-anti-PD-L1 has been described elsewhere.^{10,21} CF33-hNIS-anti-PD-L1 virus was generated by replacing the viral genes *J2R* and *F14.5L* with hNIS and anti-PD-L1 expression cassettes, respectively.

The CF33-hNIS-anti-PD-L1 clinical lots were manufactured under current good manufacturing practice (CGMP) conditions by infection of A549 cells from an established working cell bank (WCB) with CF33-hNIS and formulated in final formulation buffer consisting of 140 mM NaCl and 10 mM Tris-HCl (pH 7.8) in water for injection (WFI) tested to U.S. Pharmacopeia (USP) specifications. The clinical lots were also assessed for the presence of adventitious virus, mycoplasma, and levels of proteins and nucleic acids as well as endotoxin, and met release test specifications. Clinical-grade virus was used in the GLP study (toxicology) and in some of the non-GLP studies (in-use stability and neurotoxicity studies); laboratory stock virus (amplified in CV-1 cells and purified on sucrose gradients) was used for all other studies. Purification of virus on sucrose gradients was performed by following the protocol published from the laboratory of Bernard Moss.²²

Intracranial injection

All animal studies were conducted under City of Hope Institutional Animal Care and Use Committee approved protocol in compliance with NIH's guideline for the use of laboratory animals. Mice were injected intraperitoneally (i.p.) with ketamine/xylazine cocktail (90–150 mg/kg ketamine, 7.5–16 mg/kg xylazine), eye ointment was applied, and fur on the head was shaved. An incision of 1 cm was made using a sterile scalpel at the mid-line extending from just behind the eyes to the level of ears. Next, a hole was drilled in the skull at 1 mm lateral from the mid-line and 2 mm posterior to the lamboid suture. 1X PBS (catalog number 21-040-CV; Corning) or diluted CF33-hNIS-anti-PD-L1 virus (3 μ L per mouse) was injected using a 10 μ L Hamilton syringe with a 28G needle (0.5 μ L at 3 mm deep from the dura, 0.5 μ L at 2.75 mm deep from the dura, 0.5 μ L at 2.5 mm deep from the dura, 0.5 μ L at 2.35 mm deep from the dura, 0.5 μ L at 2.25 mm deep from the dura, and 0.5 μ L at 2.15 mm deep from dura). After retracting the needle, bone wax was used to occlude the burr hole, betadine was applied to the surgical area, and the skin was closed with skin glue. Mice were subcutaneously injected with slow-release buprenorphine. Post-surgical

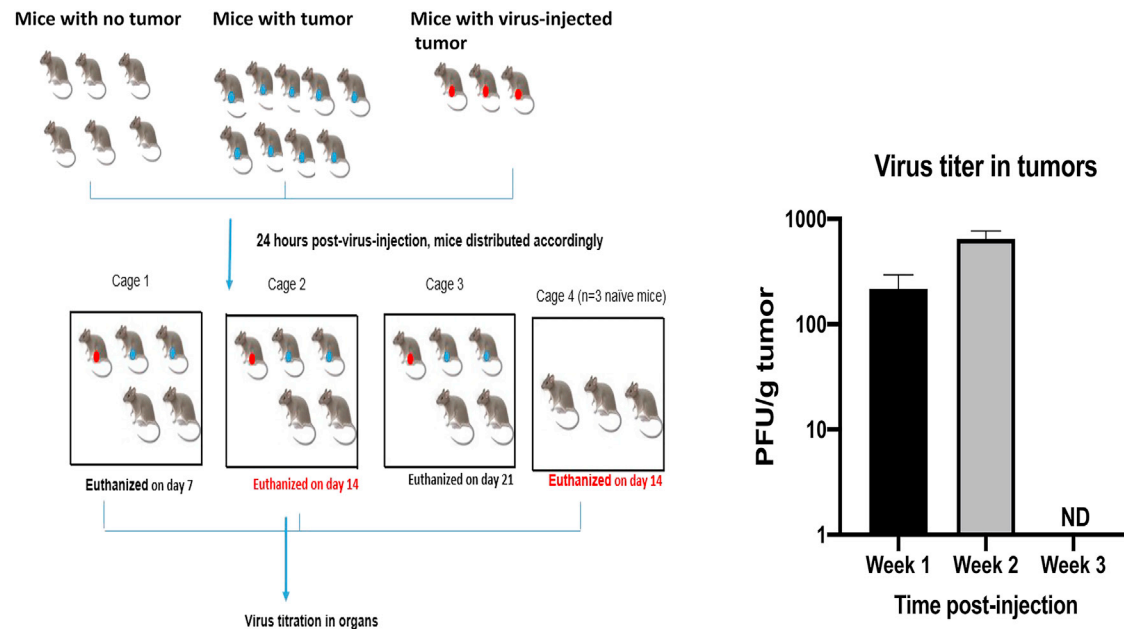


Figure 6. Assessment of risk of horizontal transmission of CF33-hNIS-anti-PD-L1

Left: experimental schema. i.t., intratumoral. Right: titer of CF33-hNIS-anti-PD-L1 in virus-injected tumors. Data represent average \pm SD. ND, not detectable.

mice were kept on a heating pad, and “Post-Op” cards were placed on the cages. Mice were monitored and weighed twice a day for the first 10 days, excluding weekends, and then once daily for the next 20 days.

Preparation of brain section

At the end of the study period, mice were euthanized using carbon dioxide (CO₂), and brain as well as other organs (including lung, liver, kidney, testes or ovary, and spleen) were harvested. Immediately after harvesting, brain tissues were placed in 10% neutral-buffered formalin and left at room temperature for 48 h for fixation. After 48 h of fixation, the tissues were sent to the Pathology Core Facility at City of Hope National Medical Center (Duarte, CA) for sectioning and hematoxylin and eosin (H&E) staining. Five sections were obtained for each brain at 5 μ m thickness, and sections 3 and 4 from each brain were H&E stained, and slides were shipped to a consultant veterinarian pathologist for assessment of the brain sections.

Virus genome analysis

Genome of CF33 was sequenced using next-generation sequencing. The genomic sequence of CF33 was aligned with nine genome sequences, including VACV strains Ankara (AS; accession number: U94848), Western Reserve (WR; NC_006,998), IHD-W clone IHDW1 (KJ125439), Lister (KX061501), Lederle-Chorioallantoic (LC), Calf-Lymph (CL), cowpox strain Brighton Red (AF482758), rabbitpox strain Utrecht (AY484669), and raccoonpox strain Herman (NC_027,213) using Kalign multiple sequence alignment (version 3).¹¹ The obtained alignments were processed using the seqinR package (<http://seqinr.r-forge.r-project.org/>) for the R environment, with trimming the gaps of CF33 sequence in the alignments and identifying the highest identity

to any parental strain. If the identities between CF33 and multiple viruses are the same, these regions will be assigned multiple origins. Identity (99.8% or higher) to the parental genomes was confirmed using Basic Local Alignment Search Tool (BLAST). The map of the genome was created using SnapGene Viewer.

Functional gene analysis

Poxvirus genes known to directly or indirectly play roles in attachment, entry, replication, and pathogenesis of virus were identified from the literature,^{11,12,23–28} and those genes in CF33 were mapped to the nine parental viruses, indicating diverse parental origins (Table 2). The functional genes in the CF33 genome were also mapped to the parental genomes to determine their origins. If the identities between CF33 and multiple viruses are the same, these regions were assigned multiple origins.

For phylogenetic analysis of viruses, we adopted PTreeRec²⁹ on the basis of genome BLAST distance to reconstruct the phylogenetic trees of CF33 and the nine parental viruses. The analysis involves three basic steps: (1) regions of maximal segment pairs (MSP) on the basis of an all-against-all pairwise comparison of genomes are located (CF33 and the nine parental genomes were applied), (2) a distance matrix is calculated from MSP scores or coverage, and (3) a phylogenetic tree is reconstructed using the neighbor-joining method.³⁰

Virus replication

In order to compare the growth kinetics of the viruses, cells (HS27, HDFa, EpH4-Ev, or NIH3T3) were seeded in 24-well plate at a density of 50,000 cells/well. On the next day, cells were infected with

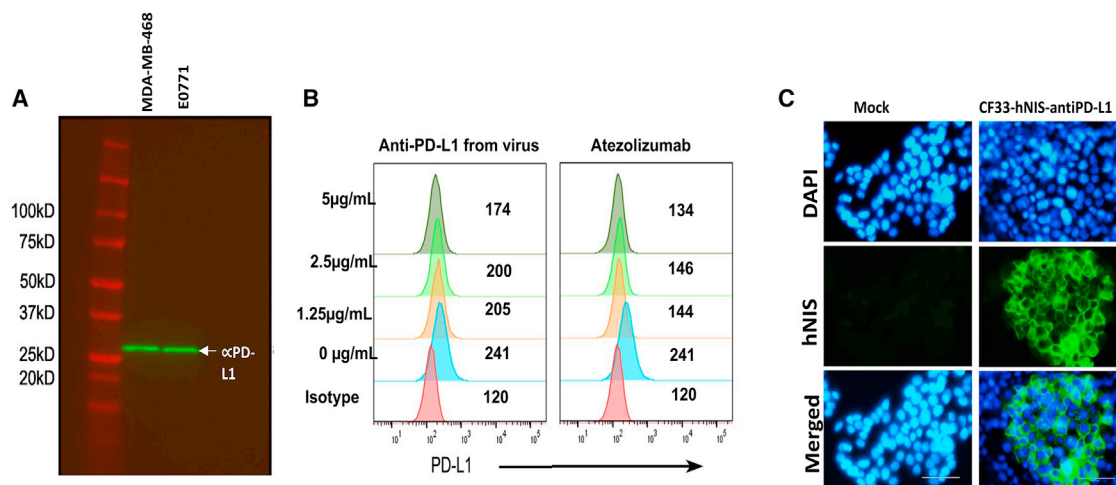


Figure 7. Detection and functionality of virus-encoded transgenes

(A) Detection of anti-PD-L1 in the supernatant of CF33-hNIS-anti-PD-L1-infected human (MDA-MB-468) and murine (E0771) TNBC cells. (B) Virus-encoded anti-PD-L1 antibody blocks surface PD-L1 binding of mouse breast cancer cell line E0771 in a dose-dependent manner. Numbers on the graphs are mean fluorescence intensity (MFI). (C) Immunofluorescent staining of hNIS protein in HT29 cells that were mock-infected (medium only) or infected with CF33-hNIS-anti-PD-L1 virus at an MOI of 0.01.

CF33-hNIS-anti-PD-L1, CF33, VACV Lister, VACV IHD, or VACV WR virus at an MOI of 0.01. After infection, plates were incubated at 37°C. Cell lysates were collected at 24, 48, and 72 h post-infection. Virus titers in the lysates as well as the initial inoculum (0 h) were determined using standard plaque assay on CV-1 cells. Fold change in virus titer (PFU/cell) was calculated relative to amount of virus used for infection (0 h).

Cytotoxicity

To determine cytotoxic potential of the viruses, 3,000 cells from each cell line (HS27, HDFa, EpH4-Ev, or NIH3T3) were seeded per well with 100 µL cell culture medium in 96-well culture plates. The following day, cells were either mock-infected (medium only) or infected with CF33-hNIS-anti-PD-L1, CF33, VACV Lister, VACV IHD, or VACV WR virus at MOIs of 0.1 and 0.01 in duplicate or triplicate. The infected cells were incubated at 37°C for 72 h. Next, CellTiter 96 AQueous (Promega) reagent was added to the cells, and 1 h later absorbance was measured at 490 nm using a plate reader (Tecan Spark). Percentage survival was calculated relative to mock-infected wells.

Risk for horizontal transmission

One day after virus injection, mice were re-caged in cage 1, cage 2, or cage 3 (as shown in Figure 6A) such that each cage had one mouse injected intratumorally with virus and four non-injected mice (two tumor-bearing and two non-tumor-bearing). The fourth cage contained three naive mice (i.e., mice with no tumors and no virus injection).

Passaging of virus

Seed stock virus was used to infect the human lung cancer cell line A549 at low MOI (about 0.01 PFU/cell). Briefly, 2 × T225 flasks were seeded with 5E06 cells/flask containing Dulbecco's modified Eagle's medium (DMEM)/F12 media supplemented with 10% fetal bovine serum

(FBS). Cells were infected with CF33-hNIS-anti-PD-L1 at an MOI of 0.01 and incubated. The media containing the virus was DMEM supplemented with 2.5% FBS. After 2 h following incubation, DMEM supplemented with 10% FBS was added to the infected cells.

Cell lysates were collected post-infection, virus was purified (passage 1) on sucrose cushion, and DNA was isolated for sequencing. Virus from P1 was used to perform the second round of infection in A549 cells to generate P2 virus, and DNA was isolated from P2 for sequencing. This process was repeated to get CF33-hNIS-anti-PD-L1 virus from up to five passages (Figure 12). At each passage, infected A549 cells were harvested and purified on a sucrose cushion per the manufacturer's protocol. DNA was harvested and sent to the Integrative Genomics Core at City of Hope National Medical Center for sequencing and analysis.

Sequencing and analysis

DNA library preparation and sequencing were performed by the Integrative Genomics Core.

Blockade bioassay of purified anti-PD-L1 antibody

Anti-PD-L1 scFv was purified using Pierce Anti-DYKDDDDK Magnetic Agarose (catalog #A36798; Thermo Fisher Scientific) per the manufacturer's protocol. Blockade bioassay of surface PD-L1 binding was performed using flow cytometry in the presence of an exogenous anti-PD-L1 antibody. Briefly, MDA-MB-468 or E0771 cells were incubated with exogenous anti-PD-L1 antibodies (purified anti-PD-L1 antibodies from virus-infected cells or positive controls: anti-human PD-L1 antibody clone 29E.2A3 or commercial anti-mouse PD-L1 antibody clone 10F.9G2 or the FDA-approved atezolizumab) for 20 min on ice. Next, PE-conjugated detection antibodies were added, that is anti-human PD-L1-PE (clone 29E.2A3) for human

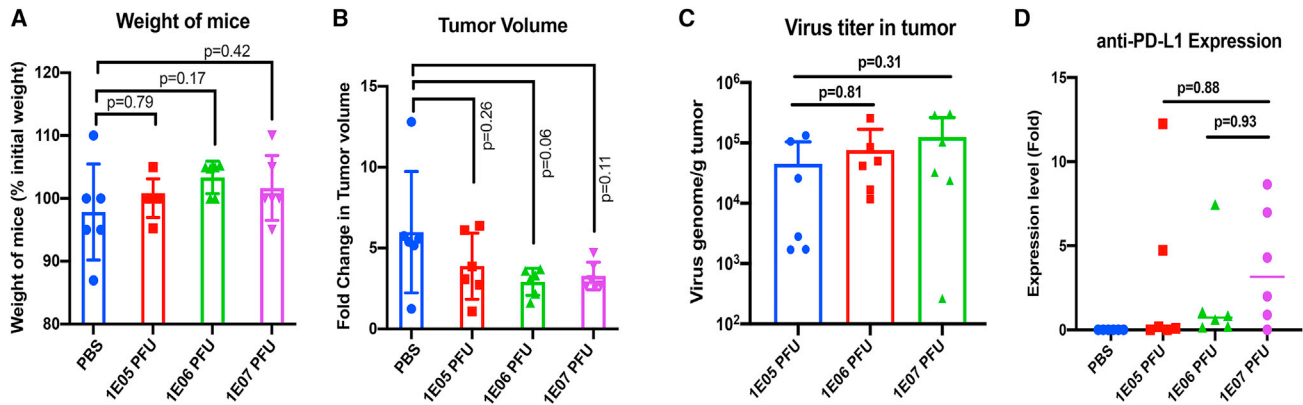


Figure 8. Safety and anti-tumor efficacy in E0771 model

(A) Mice ($n = 6/\text{group}$) were weighed immediately before virus injection and again 7 days later at the time of euthanasia. Weight of mice at the time of euthanasia was determined as percentage of the weight before virus injection. (B) Tumor volume was measured on the day of virus injection and again 7 days later on the day of euthanasia. Tumor volume was calculated using the equation: $\text{volume} = \text{length} \times (\text{breadth})^2/2$. Fold change in tumor volume was calculated by dividing the tumor volume on the day of euthanasia by the volume on the day of virus injection for individual mouse. Mean \pm SD is plotted. (C) Copy number of virus genome was determined using qPCR as described in [materials and methods](#). (D) Expression levels of anti-PD-L1 in tumors were determined using qPCR and compared among the groups treated with different doses of virus. ND, not detectable.

breast cancer cells MDA-MB-468 and anti-mouse PD-L1-PE (clone 10F.9G2) for mouse breast cancer cells E0771, and incubated on ice for 20 min. Following incubation, cells were washed with PBS containing 2% fetal bovine serum and fixed with 4% paraformaldehyde. Finally, cells were analyzed using a BD LSRFortessa Flow Cytometer, and FlowJo software was used for data analysis. Results are shown as histograms and mean fluorescence intensity (MFI).

For verification of purified antibody using western blot, purified anti-PD-L1 antibody was loaded onto Criterion Precast Gel and the Criterion Vertical Electrophoresis Cell System (Bio-Rad). Following electrophoresis, the gel was transferred to a polyvinylidene fluoride (PVDF) membrane and stained with rabbit anti-FLAG primary antibody (catalog #GTX77457; GeneTex) followed by anti-rabbit secondary antibody conjugated with the IRDye

800C (Li-CoR) and imaged using the Azure Biosystems C600 Image System. Anti-PD-L1 single-chain antibody was visualized at 26 kD ([Figure 2](#)).

Tumor models

Human TNBC cells (MDA-MB-468) were cultured in RPMI-1640 and tested for mycoplasma using the MycoAlert Mycoplasma Detection Kit as per the manufacturer's protocol (Lonza). MDA-MB-468 cells were harvested at approximately 80% confluency, using trypsin, and washed twice with 1X PBS. These cells were then counted and prepared in one part Matrigel to one part PBS at $5E06$ cells/ $50 \mu\text{L}$. Athymic (nude) mice were anesthetized using isoflurane, and sterile eye ointment was applied to their eyes to avoid dryness. A 24G needle was used to inject $50 \mu\text{L}$ cells into the abdominal mammary fat pad of each mouse within 3 h of preparation.

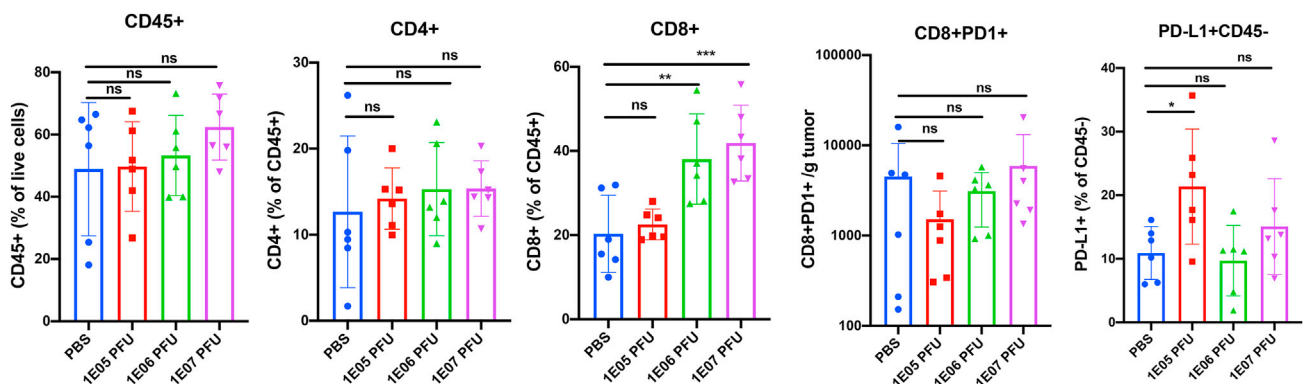


Figure 9. Immune cell analysis in E0771 model

Mice bearing E0771 tumors were injected intra-tumorally with PBS or indicated doses of the virus. One week after treatment, tumors were harvested, and immune cells were quantified using flow cytometry. Comparison of the proportion of different immune cell subsets in the tumors of mice treated with PBS or indicated doses of CF33-hNIS-anti-PD-L1. * $p < 0.05$, ** $p < 0.01$, and *** $p < 0.005$, one-way ANOVA; NS, not significant.

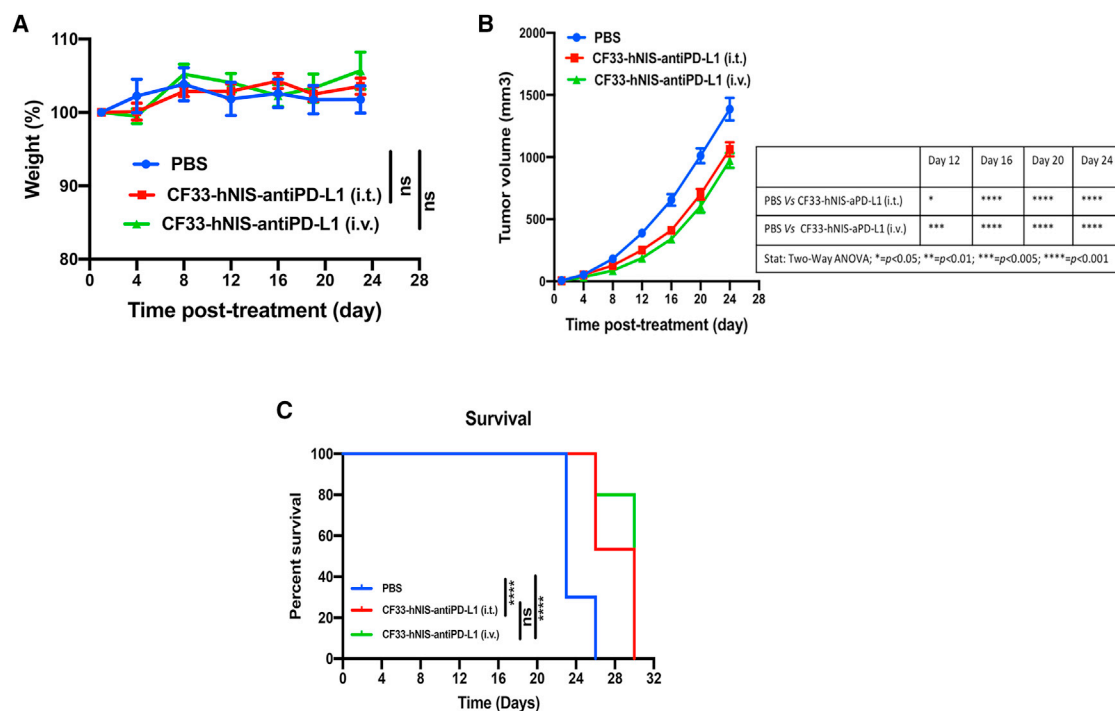


Figure 10. Safety and anti-tumor efficacy in 4T1 model

4T1 tumor-bearing mice ($n = 10$ or $n = 15$ mice/group; each mouse has 2 tumors, i.e., $n = 20$ or $n = 30$ tumors/group) were treated with PBS or virus. (A) Weight of mice was measured and compared among the treatment groups. (B) Tumors were measured twice weekly, and tumor volume was calculated using the equation: volume = length \times (breadth)²/2. Average volume \pm SEM is plotted. Statistical analysis was performed using two-way ANOVA with Dunnett's multiple-comparisons test. (C) Mice were euthanized when tumor volume reached the maximum allowed tumor burden (1,500 mm³). **** = $p < 0.0001$, log rank (Mantel-Cox) test. NS, not significant.

Murine TNBC cells E0771 were cultured in RPMI-1640 and prepared as described above. 1E05 E0771 cells were injected in anesthetized C57BL/6 mice within 3 h. Similarly, 4T1 cells were prepared in one part Matrigel to one part PBS at a concentration of 5E04 cells/50 μ L. 4T1 cells (50 μ L [5E04]) were injected subcutaneously into the abdominal mammary fat pad on both sides to generate bilateral tumors in BALB/c mice.

For all tumor models, virus treatment was initiated when the tumor volumes were in the range of 50–100 mm³.

Flow cytometry

Single cells were generated from tumors and spleens using the gentleMACS Octo Dissociator. Tumor dissociation kit (catalog #130-096-730; Miltenyi Biotec) was used per the manufacturer's protocol for tumor dissociation, and a mouse spleen dissociation kit (catalog 130-095-926; Miltenyi Biotec) was used for dissociation of spleen per the manufacturer's protocol into single-cell suspension. Several rounds of red blood cell (RBC) lysis was performed on blood and single-cell suspensions from tumors and spleens, using RBC Lysing Buffer HybriMax (catalog R7757-100ML; Sigma-Aldrich). Next, cells were washed twice with PBS and stained with Zombie UV Fixable Viability Dye (catalog #423,108; BioLegend) diluted 1:500 in PBS. Cells were then washed once with PBS, followed by another wash with fluorescence-activated cell sorting (FACS) buffer (PBS + 2% FBS). Cells were then blocked

with anti-mouse CD16/32 antibody (catalog #101,320, clone #93; BioLegend) in FACS buffer for 10 min and then stained with a cocktail of PerCP/Cyanine5.5 anti-mouse CD45 antibody (catalog #103,132, clone #30-F11; BioLegend), PE anti-mouse CD8a antibody (catalog #100,708, clone #53-6.7; BioLegend), APC anti-mouse CD279 (PD-1) antibody (catalog #135,210, clone #29F.1A12; BioLegend), PE/Cyanine7 anti-mouse CD274 (B7-H1, PD-L1) antibody (catalog #124,314, clone #10F.9G2; BioLegend), and APC/Cyanine7 anti-mouse CD4 antibody (catalog #100,526, clone #RM4-5; BioLegend) antibody for 20 min at room temperature in the dark. After staining, cells were fixed with 4% paraformaldehyde and stored at 4°C overnight. The following day, samples were run on a BD LSRFortessa. FlowJo software was used to analyze the flow cytometry data.

qPCR for quantification of virus and anti-PD-L1

Frozen tumor samples were divided into two halves; one-half was weighed and used for RNA isolation using the RNeasy Mini Kit (catalog #74,104; Qiagen), and another half was homogenized in RIPA buffer for western blot analysis. Next, cDNA was synthesized using 1,000 ng RNA using the QuantiTect Reverse Transcription Kit (catalog #205311; Qiagen) following the manufacturer's instructions. cDNA was synthesized in a total volume of 20 μ L, of which 4 μ L was used to run qPCR using TaqMan-based assay. Primers-probe specific for the viral gene *F4L* was used for quantification of virus genome, and primers-probe specific for

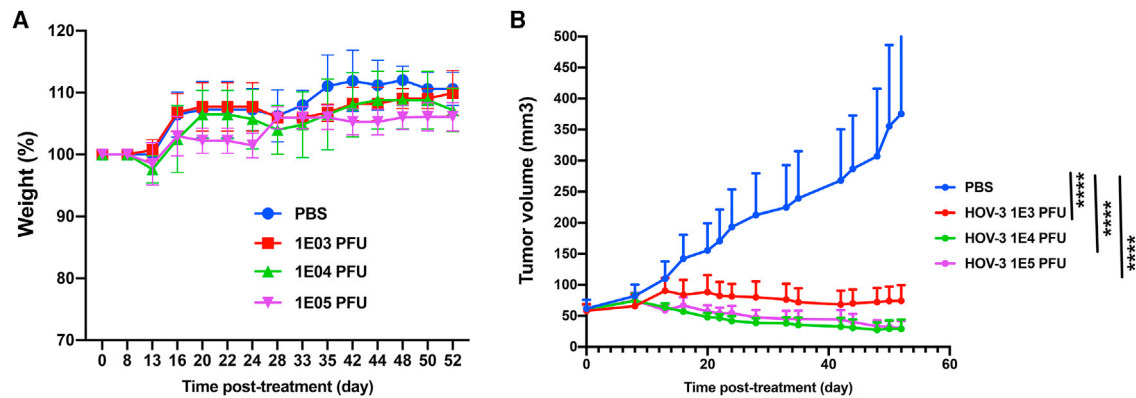


Figure 11. Safety and anti-tumor efficacy in a xenograft model

(A) Mice ($n = 5/\text{group}$) were weighed two or three times a week, and the average body weight for each group \pm SEM is plotted. (B) Tumors were measured two to three times a week using digital calipers, and tumor volume was calculated using the equation: $\text{volume} = \text{length} \times (\text{breadth})^2/2$. Average volume \pm SEM is plotted. **** $p < 0.0001$, two-way ANOVA with Dunnett's multiple-comparisons test.

the anti-PD-L1 gene spanning the FLAG tag sequence was used for detection of virus-encoded anti-PD-L1. Primers-probe set specific for mouse GAPDH was used as an internal control for further normalization of the data. All primers and probes, except for GAPDH, were self-designed and purchased from Integrated DNA Technologies. Primers-probe set for GAPDH was purchased from Qiagen. Ct values for GAPDH were used for normalization of anti-PD-L1 expression levels.

To quantify virus genome copy number, a standard curve was generated using a known amount plasmid DNA-containing viral sequence (*F4L* gene). Number of virus genome was calculated on the basis of the standard curve generated using the built-in function of qPCR machine.

To determine the stability of CF33-hNIS-anti-PD-L1 at room temperature compared with ice, two vials of CF33-hNIS-anti-PD-L1 virus (one vial at a concentration of 1×10^8 PFU/mL and one vial at a concentration of 1×10^6 PFU/mL) were removed from the -80°C freezer

and thawed at room temperature. After thawing, each vial of virus was sonicated for 1 min in ice water, and 50 μL aliquots were taken from each vial for immediate titration, which would be used as the control. The remaining virus at each concentration were divided into two microcentrifuge tubes (450 $\mu\text{L}/\text{tube}$), and one tube was left at room temperature and another tube was placed on ice. From each tube, aliquots of 50 μL virus were taken at 30 min intervals for up to 4 h, and the aliquots of virus were used immediately to infect CV-1 cells for titration at each time point. Forty-eight hours after infection of CV-1 cells, plaques were counted, and titers of virus at each time point were determined using viral plaque assay on CV-1 cells and plotted.

Stability of CF33-hNIS-anti-PD-L1 after freeze-thaw cycles

Two vials of CF33-hNIS-anti-PD-L1 virus at a concentration of 1E08 or 1E06 PFU/mL were removed from the -80°C freezer and thawed for either 30 min or 1 h at room temperature. After thawing, an aliquot of 50 μL was taken from each vial and used immediately for infecting CV-1 cells, and the original vials were immediately returned

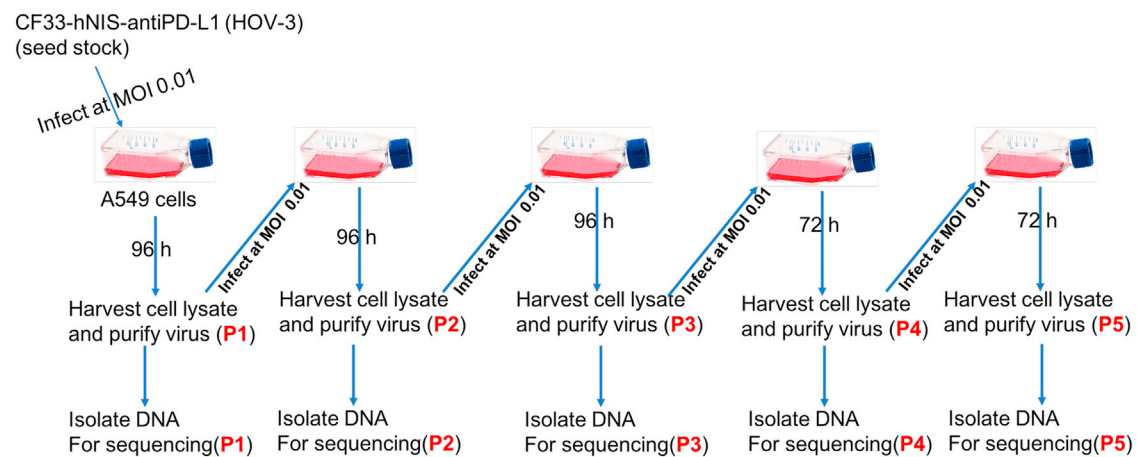


Figure 12. Schema showing serial passaging of CF33-hNIS-anti-PD-L1 and DNA isolation for sequencing

to -80°C freezer. The vials were kept in the -80°C freezer for at least 1 h and again thawed for 30 min or 1 h at room temperature, and aliquots were taken and immediately used to infect CV-1 cells. These freeze-thaw cycles were continued for up to 5 cycles, and virus titers were determined after each thaw by plaque assay on CV-1 cells.

Compatibility of CF33-hNIS-anti-PD-L1 with syringe and needle

Vials containing 1 mL CF33-hNIS-anti-PD-L1 virus (lab stocks) at a concentration of $1\text{E}08$ or $1\text{E}06$ PFU/mL were taken out of the -80°C freezer and thawed at room temperature. The stocks were then diluted 1:100 with PBS to obtain $1\text{E}06$ or $1\text{E}04$ PFU/mL. Next, 10 mL of diluted viruses were loaded in 10 mL sterile syringes (catalog #309604, lot #6291821; BD Biosciences) fitted with sterile 25G needles (catalog #305125, lot #0274523; BD Biosciences). The plunger of the syringe was slowly pushed to eject virus solution from the syringe, and the ejected viruses were collected in a 15 mL conical tube and were immediately used for titration by plaque assay.

SUPPLEMENTAL INFORMATION

Supplemental information can be found online at <https://doi.org/10.1016/j.omtm.2021.12.002>.

ACKNOWLEDGMENTS

S.C. is supported by research grant from the California Breast Cancer Research Program (CBCRP).

AUTHOR CONTRIBUTIONS

S.C., A.Y., Z.Z., J.L., H.V., S.K., and T.O. performed the experiments. Y.Z. and X.W. performed sequencing and bio-informatics analyses. S.C., Y.W., S.G.W., S.F., L.C., M.C., N.E., and Y.F. were involved in study design. S.C. wrote the manuscript.

DECLARATION OF INTERESTS

Y.F. is an adviser to Imugene Ltd. and receives royalties from Imugene and Merck. S.C. is a consultant to Imugene Ltd. All other authors declare no competing interests.

REFERENCES

- Chaurasiya, S., Fong, Y., and Warner, S.G. (2021). Oncolytic virotherapy for cancer: clinical experience. *Biomedicines* 9. <https://doi.org/10.3390/biomedicines9040419>.
- Conry, R.M., Westbrook, B., McKee, S., and Norwood, T.G. (2018). Talimogene laherparepvec: first in class oncolytic virotherapy. *Hum. Vaccin. Immunother.* 14, 839–846. <https://doi.org/10.1080/21645515.2017.1412896>.
- Kaufman, H.L., Kohlhapp, F.J., and Zloza, A. (2016). Oncolytic viruses: a new class of immunotherapy drugs. *Nat. Rev. Drug Discov.* 15, 660. <https://doi.org/10.1038/nrd.2016.178>.
- Chaurasiya, S., Chen, N.G., and Fong, Y. (2018). Oncolytic viruses and immunity. *Curr. Opin. Immunol.* 51, 83–90. <https://doi.org/10.1016/j.coi.2018.03.008>.
- Puzanov, I., Milhem, M.M., Minor, D., Hamid, O., Li, A., Chen, L., Chastain, M., Gorski, K.S., Anderson, A., Chou, J., et al. (2016). Talimogene laherparepvec in combination with ipilimumab in previously untreated, unresectable stage IIIB–IV melanoma. *J. Clin. Oncol.* 34, 2619–2626. <https://doi.org/10.1200/JCO.2016.67.1529>.
- Ribas, A., Dummer, R., Puzanov, I., VanderWalde, A., Andtbacka, R.H.I., Michielin, O., Olszanski, A.J., Malvey, J., Cebon, J., Fernandez, E., et al. (2017). Oncolytic virotherapy promotes intratumoral T cell infiltration and improves anti-PD-1 immunotherapy. *Cell* 170, 1109–1119 e1110. <https://doi.org/10.1016/j.cell.2017.08.027>.
- Andrews, A. (2015). Treating with checkpoint inhibitors-figure \$1 million per patient. *Am. Health Drug Benefits* 8, 9.
- Orloff, M. (2016). Spotlight on talimogene laherparepvec for the treatment of melanoma lesions in the skin and lymph nodes. *Oncolytic Virother.* 5, 91–98. <https://doi.org/10.2147/OV.S99532>.
- Woo, Y., Zhang, Z., Yang, A., Chaurasiya, S., Park, A.K., Lu, J., Kim, S.I., Warner, S.G., Von Hoff, D., and Fong, Y. (2020). Novel chimeric immuno-oncolytic virus CF33-hNIS-antiPDL1 for the treatment of pancreatic cancer. *J. Am. Coll. Surg.* <https://doi.org/10.1016/j.jamcollsurg.2019.12.027>.
- Chaurasiya, S., Chen, N.G., Lu, J., Martin, N., Shen, Y., Kim, S.I., Warner, S.G., Woo, Y., and Fong, Y. (2019). A chimeric poxvirus with J2R (thymidine kinase) deletion shows safety and anti-tumor activity in lung cancer models. *Cancer Gene Ther.* <https://doi.org/10.1038/s41417-019-0114-x>.
- Lassmann, T. (2019). Kalign 3: multiple sequence alignment of large data sets. *Bioinformatics.* <https://doi.org/10.1093/bioinformatics/btz795>.
- Johnston, J.B., and McFadden, G. (2004). Technical knockout: understanding poxvirus pathogenesis by selectively deleting viral immunomodulatory genes. *Cell. Microbiol.* 6, 695–705. <https://doi.org/10.1111/j.1462-5822.2004.00423.x>.
- Dohm, J.C., Peters, P., Stralis-Pavese, N., and Himmelbauer, H. (2020). Benchmarking of long-read correction methods. *NAR Genom. Bioinform.* 2, lqaa037. <https://doi.org/10.1093/nargab/lqaa037>.
- Israely, T., Paran, N., Erez, N., Cherry, L., Tamir, H., Achdout, H., Politi, B., Israeli, O., Zaide, G., Cohen-Gihon, I., et al. (2019). Differential response following infection of mouse CNS with virulent and attenuated vaccinia virus strains. *Vaccines (Basel)* 7. <https://doi.org/10.3390/vaccines7010019>.
- Li, Z., Rubin, S.A., Taffs, R.E., Merchinsky, M., Ye, Z., and Carbone, K.M. (2004). Mouse neurotoxicity test for vaccinia-based smallpox vaccines. *Vaccine* 22, 1486–1493. <https://doi.org/10.1016/j.vaccine.2003.10.022>.
- Chaurasiya, S., Yang, A., Kang, S., Lu, J., Kim, S.I., Park, A.K., Sivanandam, V., Zhang, Z., Woo, Y., Warner, S.G., and Fong, Y. (2020). Oncolytic poxvirus CF33-hNIS-DeltaF14.5 favorably modulates tumor immune microenvironment and works synergistically with anti-PD-L1 antibody in a triple-negative breast cancer model. *Oncoimmunology* 9, 1729300. <https://doi.org/10.1080/2162402X.2020.1729300>.
- Flores, E.B., Aksoy, B.A., and Bartee, E. (2020). Initial dose of oncolytic myxoma virus programs durable antitumor immunity independent of in vivo viral replication. *J. Immunother. Cancer* 8. <https://doi.org/10.1136/jitc-2020-000804>.
- Pugalenti, A., Mojica, K., Ady, J.W., Johnsen, C., Love, D., Chen, N.G., Aguilar, R.J., Szalay, A.A., and Fong, Y. (2015). Recombinant vaccinia virus GLV-1h68 is a promising oncolytic vector in the treatment of cholangiocarcinoma. *Cancer Gene Ther.* 22, 591–596. <https://doi.org/10.1038/cgt.2015.60>.
- Brun, J., Mahoney, D.J., Le Boeuf, F., Lefebvre, C., Sanaei, C.A., Falls, T., McCart, J.A., and Stojdl, D.F. (2013). Oncolytic Vaccinia virus safely and effectively treats skin tumors in mouse models of xeroderma pigmentosum. *Int. J. Cancer* 132, 726–731. <https://doi.org/10.1002/ijc.27695>.
- Guse, K., Sloniecka, M., Diaconu, I., Ottolino-Perry, K., Tang, N., Ng, C., Le Boeuf, F., Bell, J.C., McCart, J.A., Ristimaki, A., et al. (2010). Antiangiogenic arming of an oncolytic vaccinia virus enhances antitumor efficacy in renal cell cancer models. *J. Virol.* 84, 856–866. <https://doi.org/10.1128/JVI.00692-09>.
- O'Leary, M.P., Choi, A.H., Kim, S.I., Chaurasiya, S., Lu, J., Park, A.K., Woo, Y., Warner, S.G., Fong, Y., and Chen, N.G. (2018). Novel oncolytic chimeric orthopoxvirus causes regression of pancreatic cancer xenografts and exhibits abscopal effect at a single low dose. *J. Transl. Med.* 16, 110. <https://doi.org/10.1186/s12967-018-1483-x>.
- Cotter, C.A., Earl, P.L., Wyatt, L.S., and Moss, B. (2015). Preparation of cell cultures and vaccinia virus stocks. *Curr. Protoc. Microbiol.* 39, 14A.13.11–14A.13.18. <https://doi.org/10.1002/9780471729259.mc14a03s39>.
- Moss, B. (2013). Poxvirus DNA replication. *Cold Spring Harb. Perspect. Biol.* 5. <https://doi.org/10.1101/cshperspect.a010199>.
- Johnston, J.B., and McFadden, G. (2003). Poxvirus immunomodulatory strategies: current perspectives. *J. Virol.* 77, 6093–6100. <https://doi.org/10.1128/jvi.77.11.6093-6100.2003>.

25. Shchelkunov, S.N. (2012). Orthopoxvirus genes that mediate disease virulence and host tropism. *Adv. Virol.* 2012, 524743. <https://doi.org/10.1155/2012/524743>.
26. Seet, B.T., Johnston, J.B., Brunetti, C.R., Barrett, J.W., Everett, H., Cameron, C., Sypula, J., Nazarian, S.H., Lucas, A., and McFadden, G. (2003). Poxviruses and immune evasion. *Annu. Rev. Immunol.* 21, 377–423. <https://doi.org/10.1146/annurev.immunol.21.120601.141049>.
27. McFadden, G. (2005). Poxvirus tropism. *Nat. Rev. Microbiol.* 3, 201–213. <https://doi.org/10.1038/nrmicro1099>.
28. Werden, S.J., Rahman, M.M., and McFadden, G. (2008). Poxvirus host range genes. *Adv. Virus Res.* 71, 135–171. [https://doi.org/10.1016/S0065-3527\(08\)00003-1](https://doi.org/10.1016/S0065-3527(08)00003-1).
29. Deng, R., Huang, M., Wang, J., Huang, Y., Yang, J., Feng, J., and Wang, X. (2006). PTreeRec: phylogenetic Tree Reconstruction based on genome BLAST distance. *Comput. Biol. Chem.* 30, 300–302. <https://doi.org/10.1016/j.compbiolchem.2006.04.003>.
30. Tamura, K., Nei, M., and Kumar, S. (2004). Prospects for inferring very large phylogenies by using the neighbor-joining method. *Proc. Natl. Acad. Sci. U S A* 101, 11030–11035. <https://doi.org/10.1073/pnas.0404206101>.